Electronic Supplementary Material (ESI) for Journal of Materials Chemistry A.

Controllable Interfacial Electron Transfer Induced by Heterointerfaced Sulfur-based Catalysts with Lower Electronegative Anion for Boosted Hydrogen Evolution Reaction in Universal pH Range

Dawei Chu [a, b, ‡], Xiaoling Wei [c, ‡], Xiumei Song [d, f ‡], Zhen Zhang [e], Lichao Tan [a, f *], Huiyuan Ma [a, *], Haijun Pang [a], Xin Wang [c, f], and Zhongwei Chen [e, *]

[a] School of Materials Science and Chemical Engineering, Harbin University of Science and Technology, Harbin 150040, P. R. China

[b] Department of Materials Science and Engineering, National University of Singapore, Singapore 117574, Singapore

[c] South China Academy of Advanced Optoelectronics & International Academy of Optoelectronics at Zhaoqing, South China Normal University, Guangdong 510006, China

[d] State Key Laboratory of Urban Water Resource and Environment, School of Environment, Harbin Institute of Technology, Harbin, 150090, P. R. China

[e] Department of Chemical Engineering, University of Waterloo, Waterloo, ON N2L 3G1, Canada

[f] Carbon Neutral Research Institute, Zhejiang Wanli University, Ningbo 315100, P.R. China

E-mail: lctan@hrbust.edu.cn (L. Tan); mahy017@nenu.edu.cn (H. Ma); zhwchen@uwaterloo.ca (Z. Chen)

‡ These authors contributed equally to this work.

1. Experimental section

1.1 Chemicals

All the chemical reagents; nickel nitrate hexahydrate ($Ni(NO_3)_2 \cdot 6H_2O$) (Shanghai Dibo Chemicals Technology Co., Ltd. ≥ 98.0%), Cobalt nitrate ($Co(NO_3)_2 \cdot 6H_2O$) (Shanghai Aladdin Biochemical Technology Co., Ltd. 99.0%), 2-methylimidazole (Shanghai Aladdin Biochemical Technology Co., Ltd. 98.0%), Thioacetamide (TAA) (CH_3CSNH_2) (Shanghai Aladdin Biochemical Technology Co., Ltd. ≥ 99.0%) sodium hypophosphite ($NaH_2PO_2 \cdot H_2O$) (Shanghai Aladdin Biochemical Technology Co., Ltd. ≥ 99.0%), absolute ethanol (Tianli Chemical Reagent Co., Ltd. ≥ 99.7%) and deionized (DI) water were analytical grades and used directly without further purification.

1.2 Preparation detail

1.2.1 Synthesis of Co-MOF/NF sample

Co-MOF/NF sample was prepared using a dipping method. Firstly, $Co(NO_3)_2 \cdot 6H_2O$ (0.29103 g) and 2-methylimidazole (1.3136 g) were dissolved separately into DI water (40 mL), then stirred for 30 min to obtain a uniform solution and then the two solutions were mixed up. After that, the NF was transferred into the mixed solution and maintained for 4 h in the air atmosphere. After the above operation, the Co-MOF/NF was collected, washed several times with DI water and dried at 60 ^oC for 24 h.

1.2.2 Synthesis of NCL/NF sample

The NCL/NF sample was synthesized with a condensation reflow method. $Ni(NO_3)_2 \cdot 6H_2O$ (0.2 g) and Co-MOF/NF were initially dispersed into absolute ethanol (50 mL) and kept at 100 °C for 1 h. Then, the sample was cooled down to room temperature, rinsed with DI water several times and dried at 60 °C for 12 h.

1.2.3 Synthesis of NCS-X/NF sample

The NCS-X/NF sample was synthesized with a hydrothermal method. Typically, DI water (50 mL), NCL/NF and TAA were transferred into 100 mL Teflon-lined stainless-steel

autoclave, then kept at 160 °C for 4/6/10/14 h (The ratio of mass $_{NCL/NF\ -\ NF}$ and mass $_{TAA}$ is 1 : 4). After the autoclave was cooled down to room temperature, the sample was rinsed with DI water several times and dried at 60 °C for 12 h.

1.2.4 Synthesis of V_s-NCSP-X/NF sample

The NCS-X/NF and $NaH_2PO_2 \cdot H_2O$ were charged in different porcelain boats of tube furnace (The ratio of mass $_{NCS\text{-}X/NF\ -\ NF}$ and mass $_{NaH_2PO_2 \cdot H_2O}$ is 1 : 10). Before the heat treatment, nitrogen was introduced into the quartz tube at a flow rate of 200 sccm for 15 min to eliminate the remaining air. Then, the samples were subsequently calcined at 300 ^oC (with 5 ^oC/min heating rate) under nitrogen atmosphere for 2 h to form the NCSP-X/NF with S defects for electrode testing.

1.2.5 Synthesis of V_s-CSP-X/NF and CS-10/NF sample

The preparation process of V_s-CSP-10/NF is the same as V_s-NCSP-10/NF without additional $Ni(NO_3)_2 \cdot 6H_2O$. The preparation process of CS-10/NF is similar to NCS-10/NF without the addition of $Ni(NO_3)_2 \cdot 6H_2O$.

2. Materials characterization

The structure of the fabricated products was investigated using a scanning electron microscope (FE-SEM) (Hitachi, SU8000) and a transmission electron microscope (TEM) (JEOL, JEM-2010, 200 kV). Electronic paramagnetic resonance (EPR) characterization was performed using the EPRA300-9.5/12 (Bruker) electron paramagnetic resonance spectrometer. The atomic force microscope (AFM) was performed using Park systems. Raman spectra were obtained using Thermo Fischer DXR 2Xi. X-ray diffraction (XRD) analysis was performed using a powder X-ray diffraction system (Rigaku, TTR-III) equipped with Cu Kα radiation (λ = 0.15406 nm) to determine crystalline structures of the obtained samples. The X-ray photoelectron spectroscopy (XPS) measurements were performed using a Thermo ESCALAB 250Xi spectrometer with monochromated Al K_α radiation ($h\gamma$ = 1486.6 eV). All XPS spectra were calibrated according to the C 1s peak at 284.6 eV.

3. Electrochemical measurement

The electrochemical measurements were implemented using the three-electrode system on an electrochemical workstation (CHI 760E). Graphite and Hg/HgO electrodes were severed as the counter and reference electrodes, respectively. An electrode with the sample coated on NF was used as the working electrode. 1 M KOH, 0.5 M H_2SO_4 and 1 M phosphate-buffered saline (PBS) were used as electrolytes. 1 M PBS was prepared by mixing 1 M KOH and KH_2PO_4 (13.609 g, 100 mL DI water) solution until the pH value reached 7. The cyclic voltammetry (CV) curves were tested at a series of scan rates (5 mV/s, 10 mV/s, 20 mV/s, 40 mV/s, 60 mV/s, 80 mV/s, 100 mV/s). The iR-corrected linear sweep voltammetric (LSV) curves were tested at the scan rate of 5 mV/s. The Tafel slope is obtained by linearly fitting the points in the Tafel region of the LSV data. Electrochemical impedance spectroscopy (EIS) was tested from 100 kHz to 0.005 Hz. The amperometric current density-time (I-t) curves were measured at -10 mA cm^{-2}. And the measured potential *vs.* Hg/HgO was calculated to a reversible hydrogen electrode (RHE) based on the equation ($E_{RHE} = E_{Hg/HgO} + 0.0591 \times pH + 0.2415$).

4. Density functional theory calculations

Computation detail

Modelling HER: For a quantitative description of the interactions between the catalysts and adsorbed H*, the binding energy ΔE_H was defined as follows:[1]

$$\Delta E_H = E_{(catalyst+H)} - E_{(catalyst)} - 1/2E_{(H_2)} \quad (1)$$

Where (catalyst + H) refers to hydrogen adsorbed on the catalyst surface, (catalyst) refers to a clean catalyst surface, and (H_2) refers to hydrogen molecules. The hydrogen adsorption free energy was calculated at zero potential and pH=14 according to the reference.[2]

$$\Delta G_H = \Delta E_H + \Delta E_{ZPE} - T\Delta S + \Delta G_{pH} \quad (2)$$

Where ΔE_H is the hydrogen adsorption energy, ΔE_{ZPE} is the difference in zero-point energy, T is the temperature (300 K) and ΔS is the entropy change. In the alkaline environment, ΔG_{PH} should be considered and is the H^+ free energy correction by entropy:[3]

$$\Delta G_{pH} = -k_B T ln[H^+] \quad (3)$$

DFT calculation

The binding energy of NaO_2 to various substrates was calculated using the commercial Cambridge sequential total energy package program (CASTEP). Generalized gradient approximation with the Perdew-Burke-Ermzerh of functional was adopted for the total energy calculations. The ultrasoft pseudopotential was used to treat core electrons. The energy cutoff was set to 550 eV. The vacuum region between slabs is 20 Å. The Brillouin zone of the surface unit cell was sampled using Monkhorst-Pack grids, which were set as 4 × 4 × 1 for all surfaces and slabs.

5. Supporting figures

Figure S1

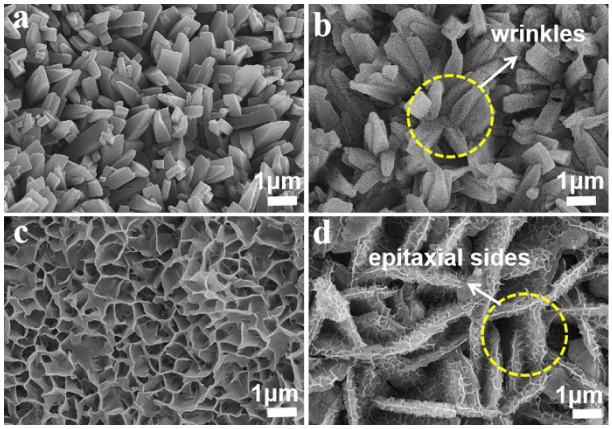

Fig. S1. SEM images of (a) Co-MOF/NF; (b) NCL/NF; (c) NCS-10/NF; (d) V_s-NCSP-10/NF.

Figure S2

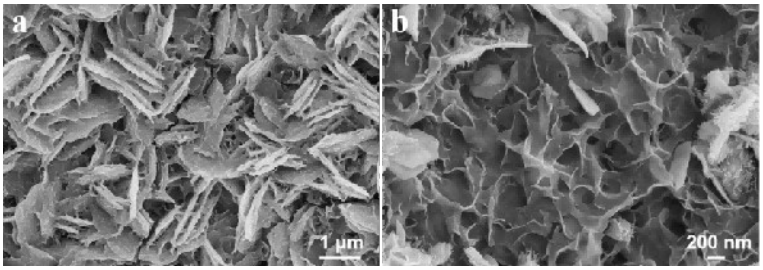

Fig. S2. SEM images of NCS-10/NF (a) $M_{NCL/NF}$: M_{TAA} = 1 : 2; (b) $M_{NCL/NF}$: M_{TAA} = 1 : 6. $M_{NCL/NF}$ devoted as the difference in mass between NCL grown on NF and pure NF; M_{TAA} devoted as the value in mass.

Figure S3

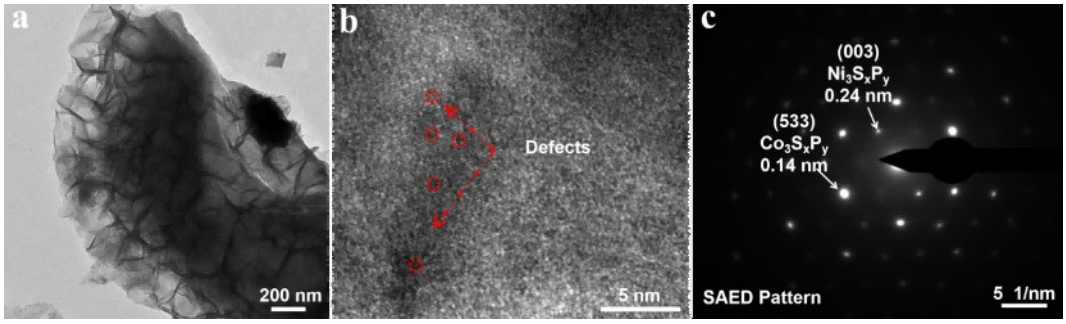

Fig. S3. TEM images of (a) V_s-NCSP-10. (b) Marked defects image. (c) SAED Pattern.

Figure S4

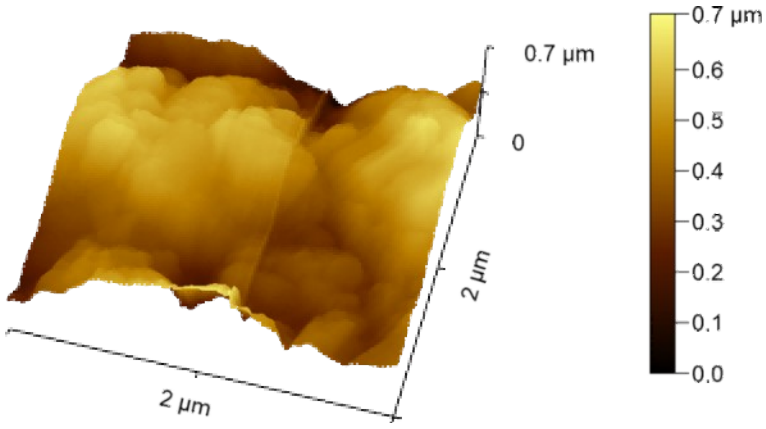

Fig. S4. AFM images of V_s-NCSP-10 sample.

Figure S5

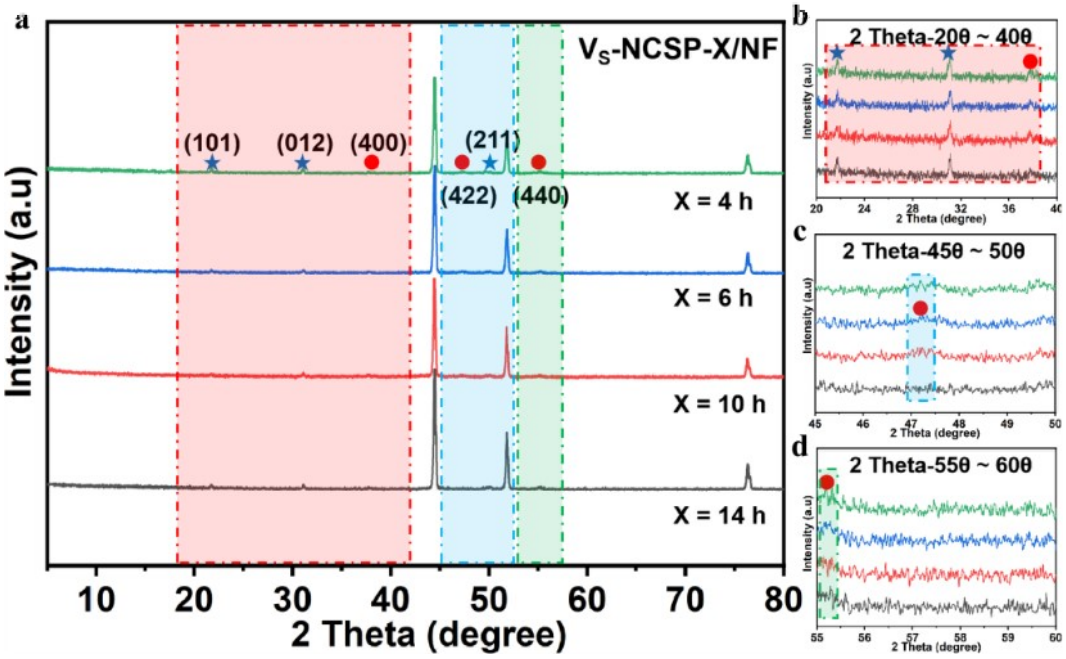

Fig. S5. XRD patterns of (a) V_s-NCSP-X/NF; Enlarged view of the part with different theta: (b) 20θ - 40θ; (c) 45θ - 50θ; (d) 55θ - 60θ.

Figure S6

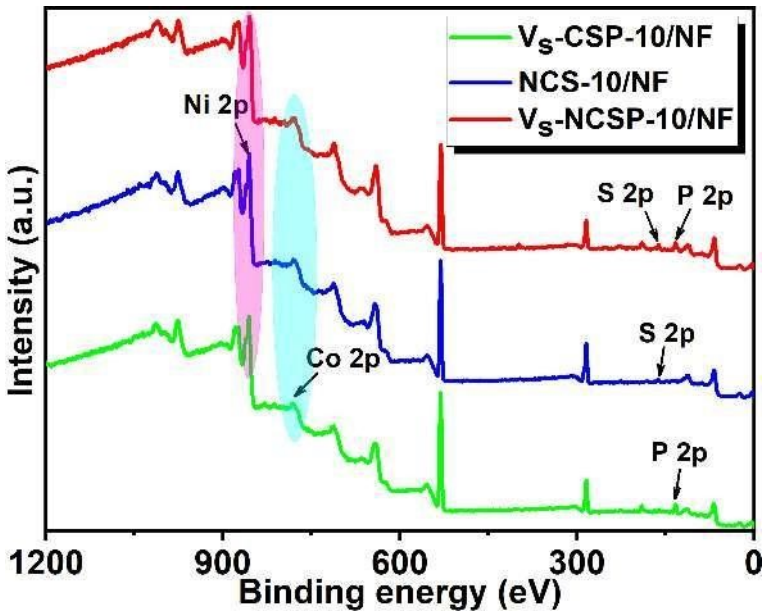

Fig. S6. Survey XPS spectra of the catalysts.

Figure S7

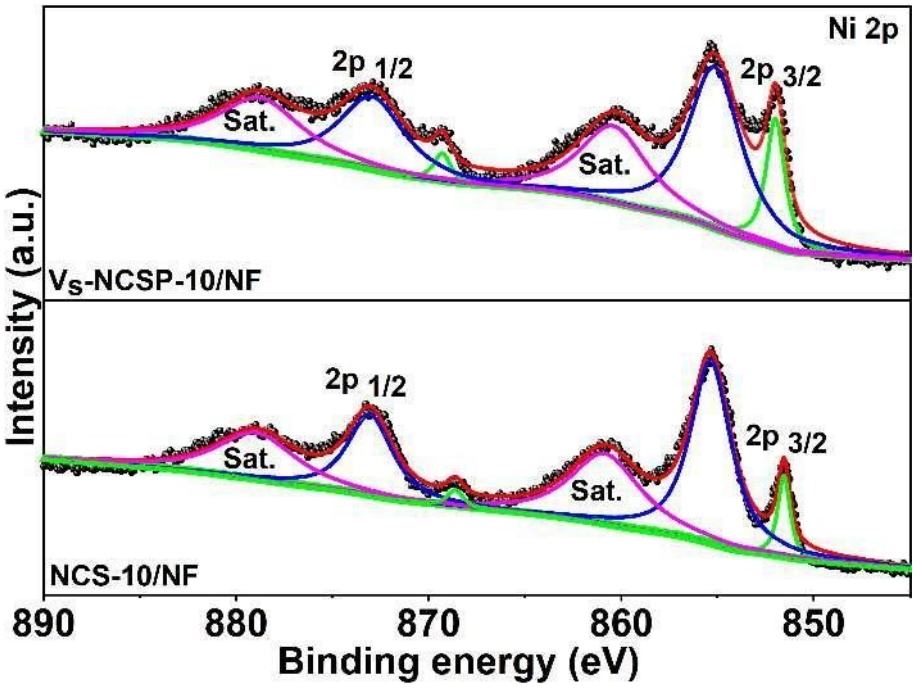

Fig. S7. Ni 2p XPS spectra of different catalysts.

Figure S8

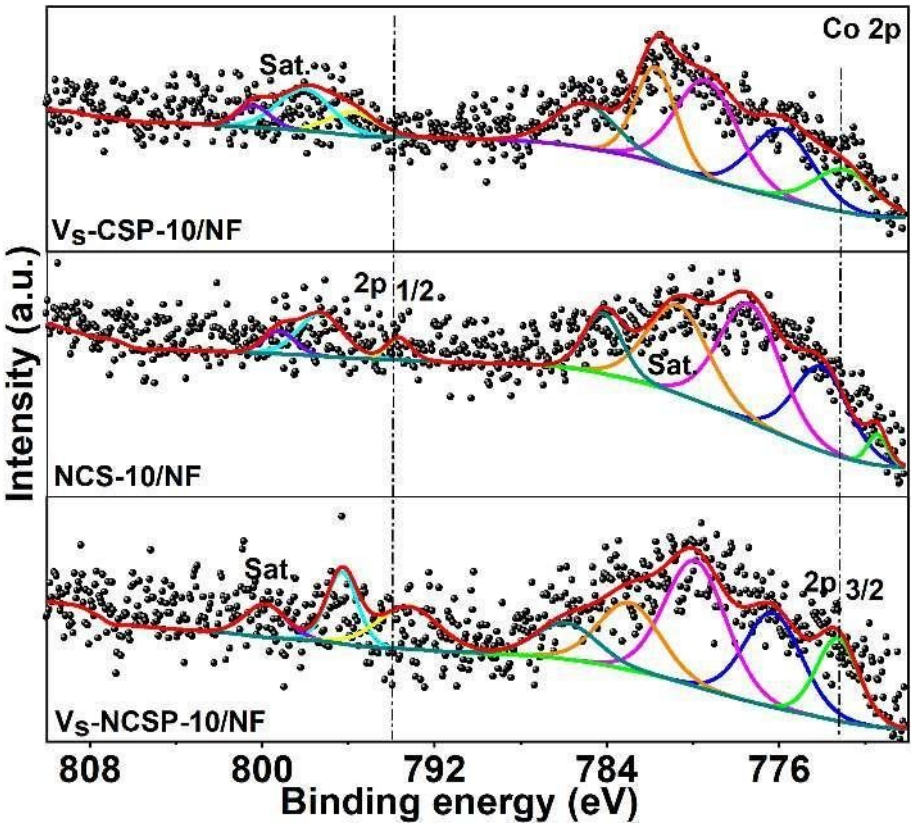

Fig. S8. Co 2p XPS spectra of different catalysts.

Figure S9

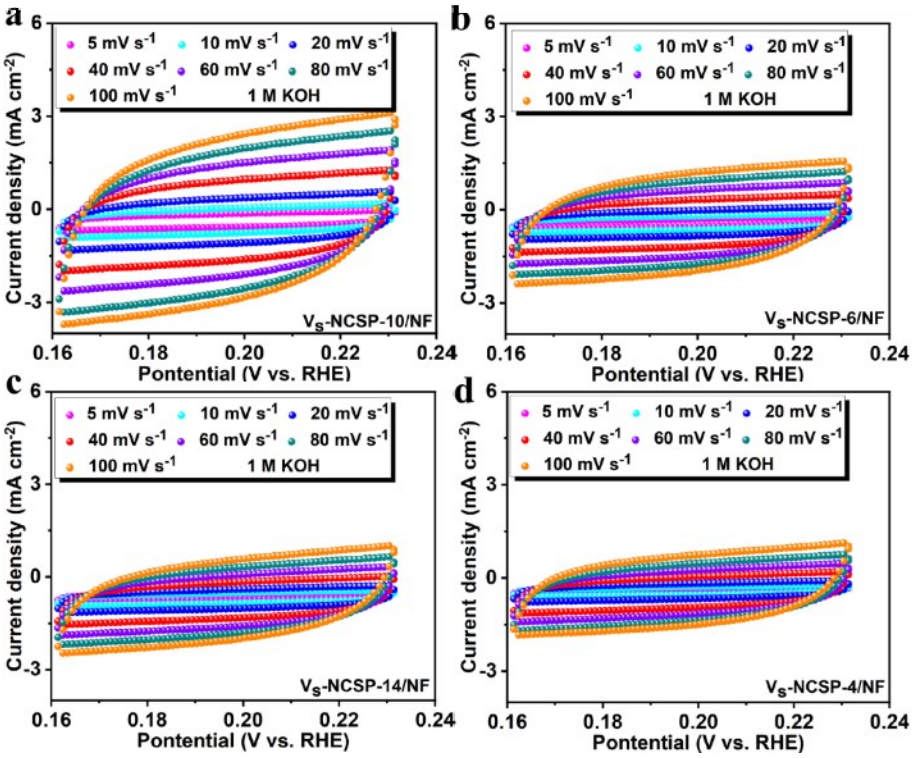

Fig. S9. The CV curves of V_s-NCSP-X/NF: (a-d) in 1 M KOH.

Figure S10

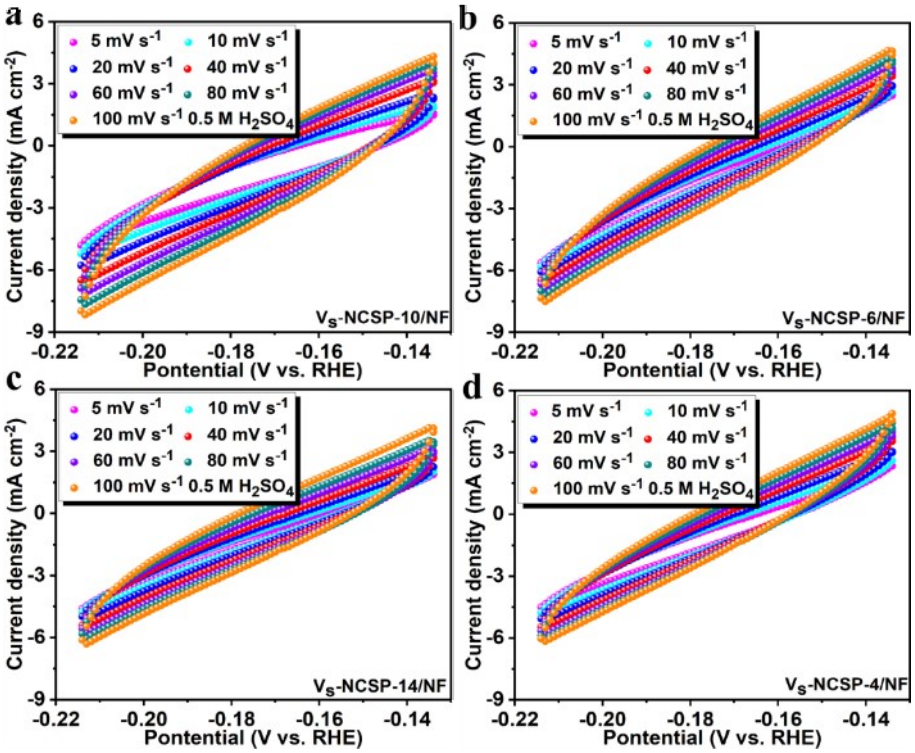

Fig. S10. The CV curves of V_s-NCSP-X/NF: (a-d) in 0.5 M H_2SO_4.

Figure S11

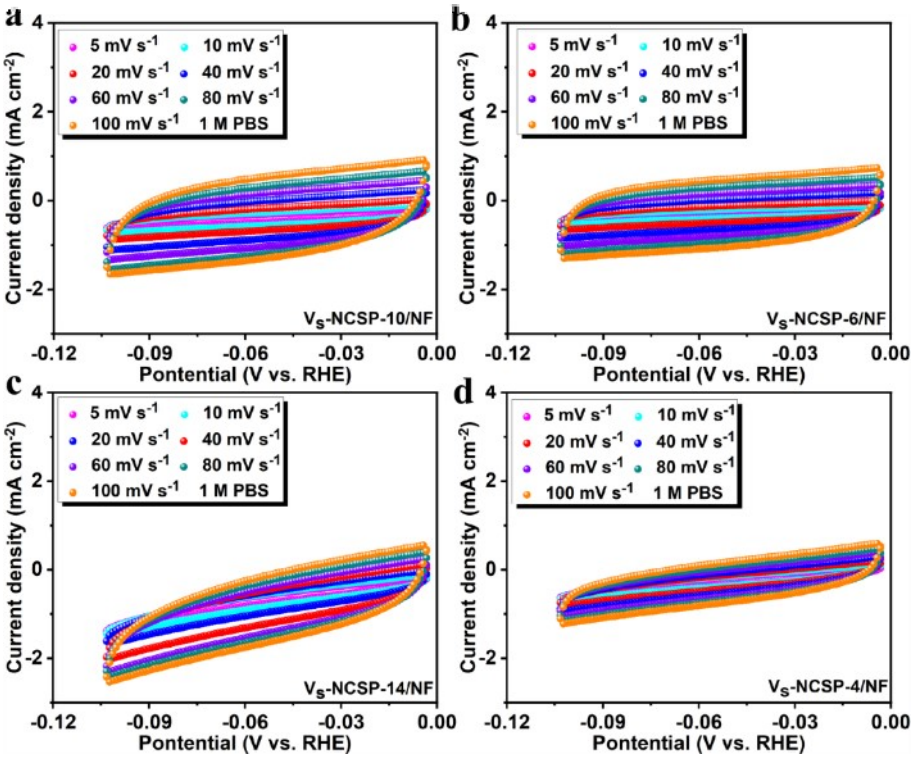

Fig. S11. The CV curves of V_s-NCSP-X/NF: (a-d) in 1 M PBS.

Figure S12

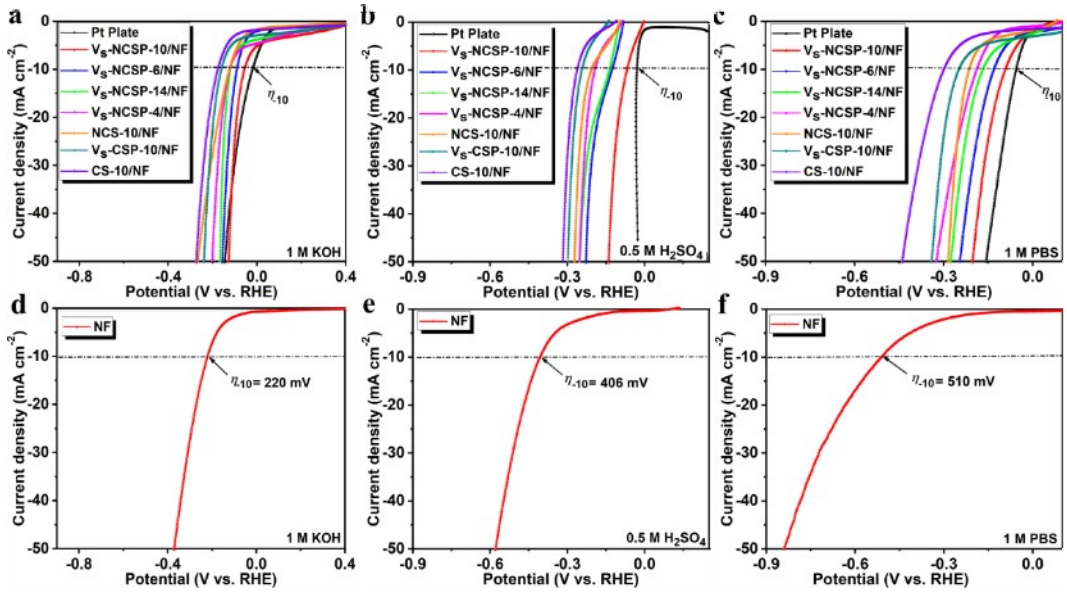

Fig. S12. The IR-corrected LSV curves of catalysts in (a) 1 M KOH, (b) 0.5 M H_2SO_4, (c) 1 M PBS. The LSV curves of NF in (d) 1 M KOH, (e) 0.5 M H_2SO_4, (f) 1 M PBS.

Figure S13

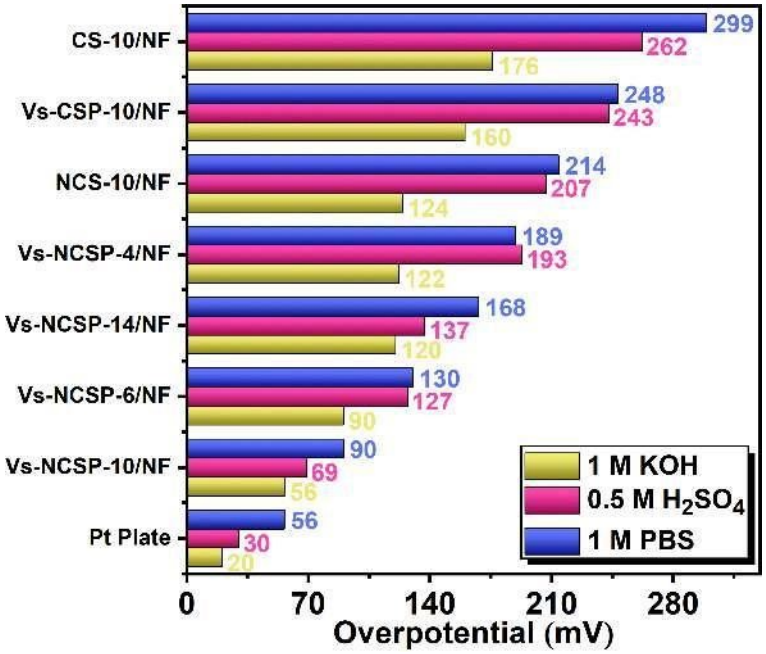

Fig. S13. The summary overpotential of this work with the different pH range at -10 mA cm^{-2}.

Figure S14

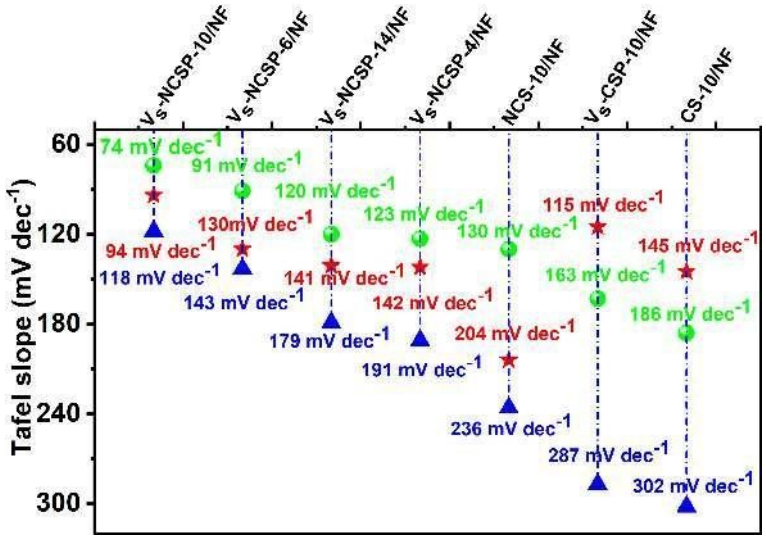

Fig. S14. The summary Tafel slope of this work at the different pH range. The green ball/red pentagon/blue triangle represents 1 M KOH, 0.5 M H_2SO_4 and 1 M PBS, respectively.

Figure S15

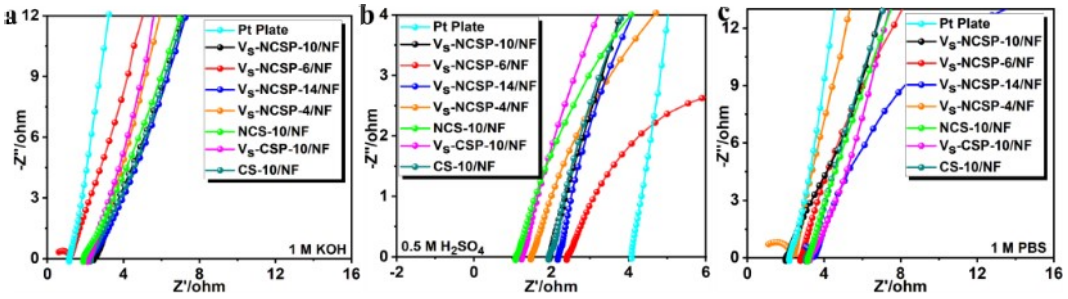

Fig. S15. EIS curves of catalysts in (a) 1 M KOH, (b) 0.5 M H_2SO_4, (c) 1 M PBS.

Figure S16

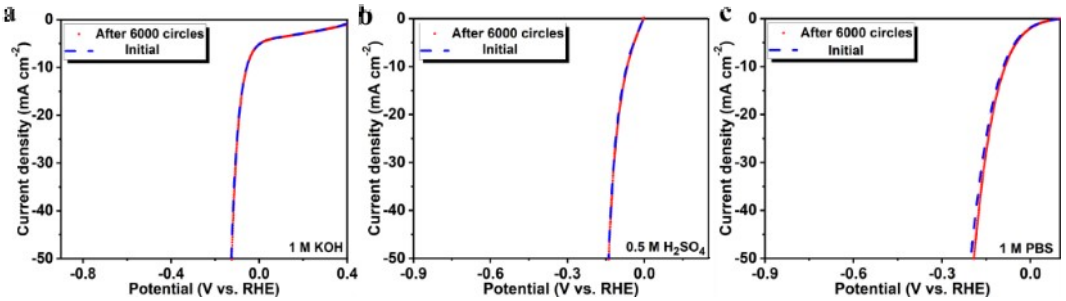

Fig. S16. The IR-corrected LSV curves of V_s-NCSP-10/NF at the initial stage and after 6000 circles with (a) 1 M KOH, (b) 0.5 M H_2SO_4, (c) 1 M PBS.

Figure S17

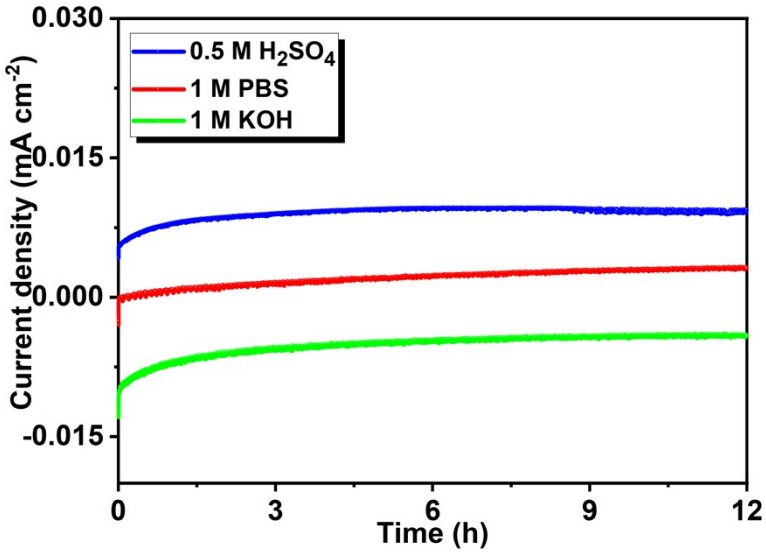

Fig. S17. Amperometric I-t curves measure of the V_s-NCSP-10/NF with the different pH range for HER.

Figure S18

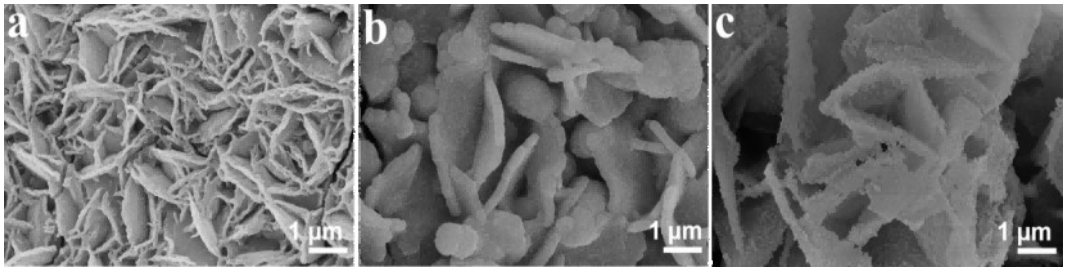

Fig. S18. The SEM images of V_s-NCSP-10/NF sample after HER process in (a) 1 M KOH, (b) 0.5 M H_2SO_4, (c) 1 M PBS.

Figure S19

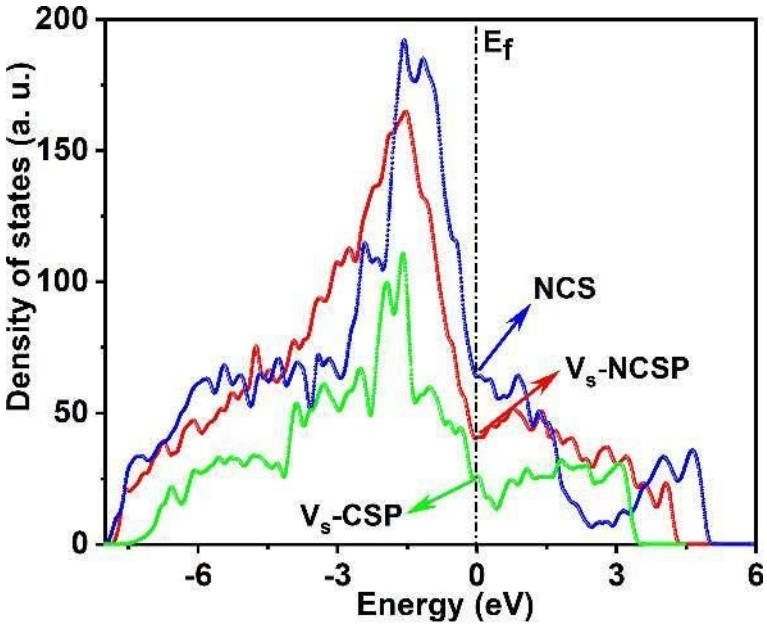

Fig. S19. Calculated density of states of NCS, V_s-NCSP and V_s-CSP. The black line denotes as the position of the Fermi energy level.

Figure S20

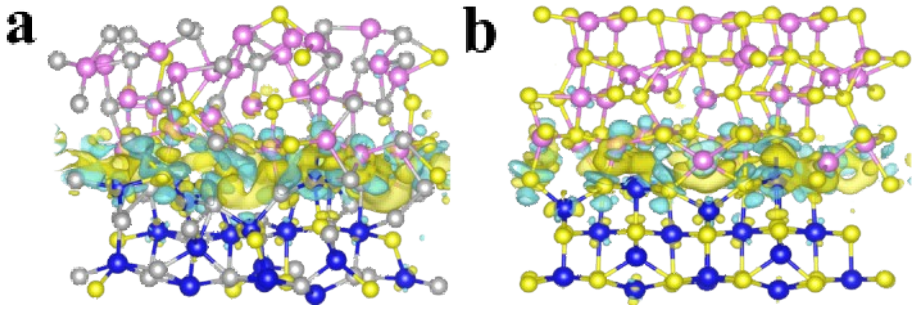

Fig. S20. Optimized charge density difference geometry of (a) V_s-NCSP, (b) NCS. The blue, pink, yellow and grey balls represent Co, Ni, S and P atoms, respectively.

Figure S21

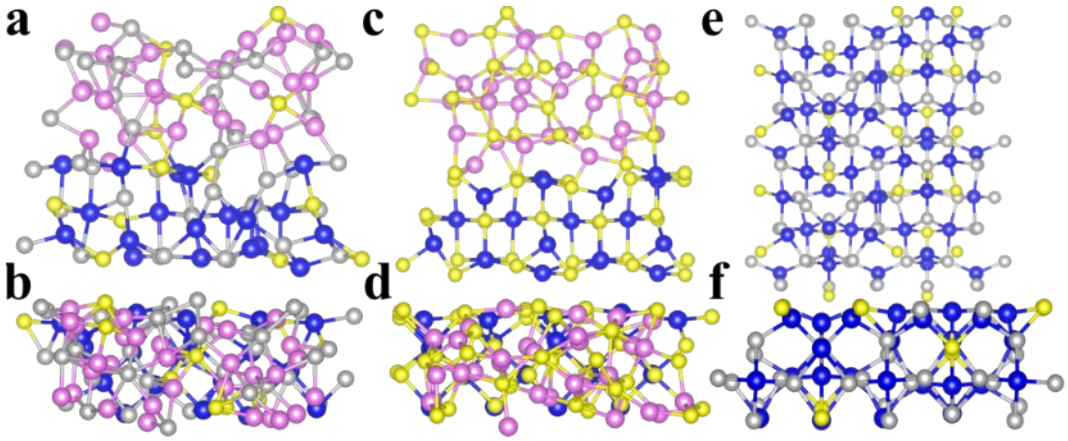

Fig. S21. The surface structure of different catalysts on various direction's view: (a, b) V_s-NCSP, (c, d) NCS, (e, f) V_s-CSP. The blue, pink, yellow and grey balls represent Co, Ni, S and P atoms, respectively.

Figure S22

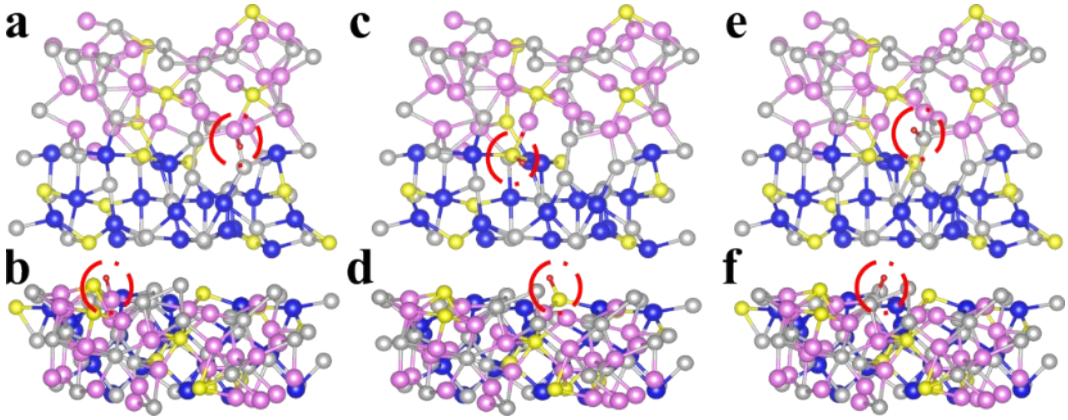

Fig. S22. The surface structure of hydrogen adsorption on different sites: (a, b) Ni site, (c, d) S site, (e, f) P site of V_s-NCSP. The blue, pink, yellow, grey and red balls represent Co, Ni, S, P and H atoms, respectively.

Figure S23

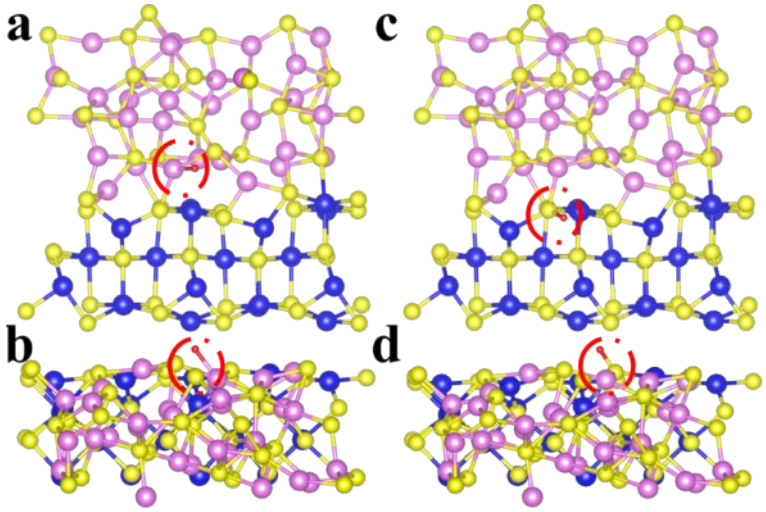

Fig. S23. The surface structure of hydrogen adsorption on different sites: (a, b) Ni site, (c, d) S site of NCS. The blue, pink, yellow and red balls represent Co, Ni, S and H atoms, respectively.

Figure S24

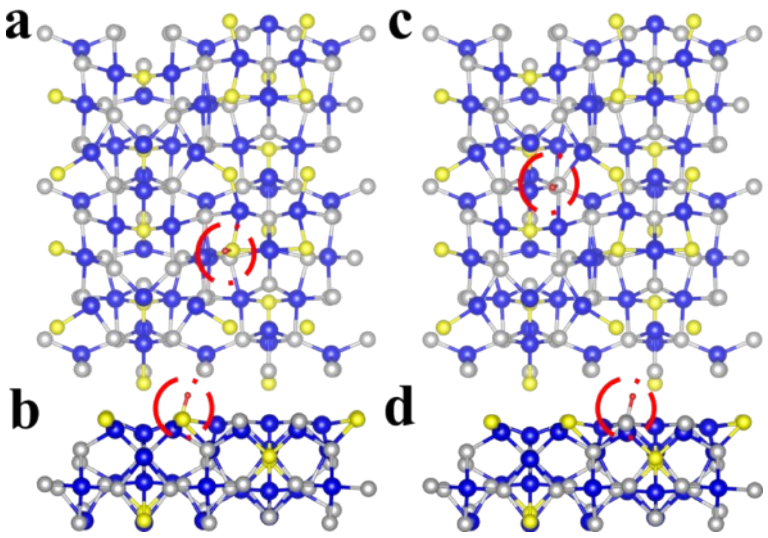

Fig. S24. The surface structure of hydrogen adsorption on different sites: (a, b) S site, (c, d) P site of V_s-CSP. The blue, yellow, grey and red balls represent Co, S, P and H atoms, respectively.

Figure S25

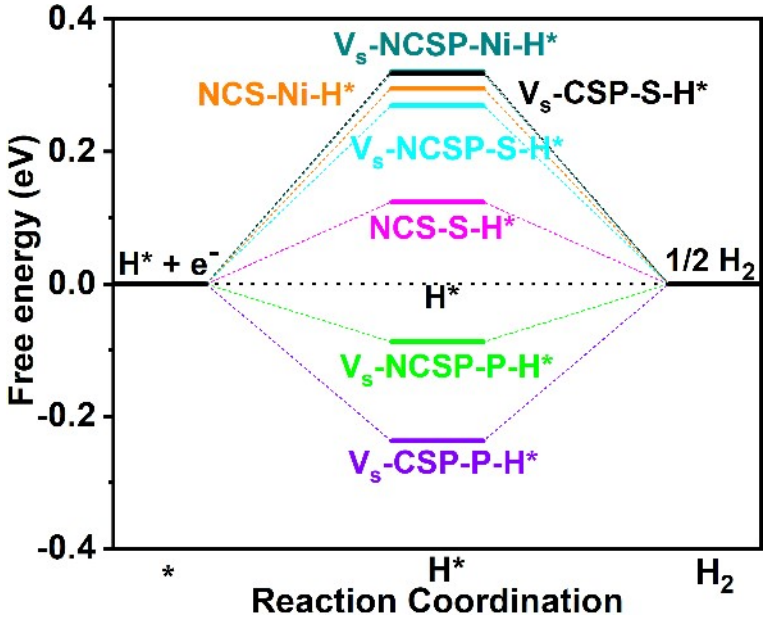

Fig. S25. Gibbs free energy (ΔG_{H^*}) on Ni/S/P sites of V_s-NCSP, NCS and V_s-CSP.

6. Supporting tables

Table S1. The content of S and P atomic originated from XPS characterization.

Catalysts	S Atomic %	P Atomic %
V_s-NCSP-X/NF	2.28	7.05
V_s-CSP-X/NF	1.78	5.86

Table S2. The survey of HER activity for catalysts in this work. (The Ni-foam has no iR-Correction)

Catalysts	Media					
	1 M KOH		**0.5 M H_2SO_4**		**1 M PBS**	
	Overpotential -10 mA cm^{-2} (mV)	Tafel (mV dec^{-1})	Overpotential -10 mA cm^{-2} (mV)	Tafel (mV dec^{-1})	Overpotential -10 mA cm^{-2} (mV)	Tafel (mV dec^{-1})
Pt plate	20	N/A	30	N/A	56	N/A
Ni-foam	220	N/A	406	N/A	510	N/A
V_s-NCSP-4/NF	122	123	193	142	189	191
V_s-NCSP-6/NF	90	91	127	130	130	143
V_s-NCSP-10/NF	56	74	69	94	90	118
V_s-NCSP-14/NF	120	120	137	141	168	179
NCS-10/NF	124	130	207	204	214	236
V_s-CSP-10/NF	160	163	243	115	248	287
CS-10/NF	176	186	262	145	299	302

Table S3. Comparison of HER activity for catalysts in this work and other reported electrocatalysts at -10 mA cm^{-2}.

Catalysts	Media			Ref.
	1 M KOH	0.5 M H_2SO_4	1 M PBS	
	Overpotential (mV)			
This Work	56	69	90	/
MoS_2/Ni_3S_2	89	N/A	N/A	4
Co-TiO_2@Ti	78	N/A	N/A	5
CoMoNiS-NF	113	103	117	6
Ni_3S_2/NF	189	N/A	N/A	7
$NiCo_2S_4$/NF	260	N/A	N/A	8
$NiCo_2S_4$/NF	137	N/A	N/A	9
Co_9S_8/Ni_3S_2	128	N/A	N/A	10
N-doped Ni_3S_2	155	N/A	N/A	11
Ni_3S_2	182	N/A	N/A	12
$NiCo_2S_4$	248	N/A	N/A	13
V-doped CoP/CC	71	N/A	123	14
Mn-CoP/Ti mesh	76	N/A	192	15
Mo-CoP/N-C	83	N/A	130	16
CoP/FeP	67.2	N/A	76.5	17
Ni-P/Ni/NF	129	83	112	18
CoSAs-MoS_2/TiN	131.9	187.5	203.4	19
Ni-doped CoP	N/A	144	N/A	20
Mn-doped CoP	N/A	178	N/A	20
Fe-doped CoP	N/A	198	N/A	20
$Zn_{0.3}Co_{2.7}S_4$	N/A	80	N/A	21
Co@N-CNTs@rGO	N/A	87	N/A	22
CoPS/N-C	N/A	80	N/A	23
FeP_2-NiP_2@P-C	N/A	117	N/A	24
Fe/Co/Ni based P	N/A	138	N/A	25
$Ni_2P_4O_{12}$	N/A	131.8	N/A	26
V-doped CoP/NF	N/A	73	N/A	27
Fe-Co_9S_8/CC	N/A	65	192	28
Ru-Ni-BDC	N/A	N/A	219	29

7. Supplementary references

1 J. Greeley, T.F. Jaramillo, J. Bonde, I.B. Chorkendorff, J.K. Norskov, *Nat. Mater.*, 2006, **5**, 909-913.

2 Y. Hou, M. Qiu, T. Zhang, X. Zhuang, C.S. Kim, C. Yuan, X. Feng, *Adv. Mater.*, 2017, **29**, 1701589.

3 Q. Zhou, Z. Shen, C. Zhu, J. Li, Z. Ding, P. Wang, F. Pan, Z. Zhang, H. Ma, S. Wang, H. Zhang, *Adv. Mater.*, 2018, **30**, 1800140.

4 L. Zhang, Y. Zheng, J. Wang, Y. Geng, B. Zhang, J. He, J. Xue, T. Frauenheim, M. Li, *Small*, 2021, **17**, 2006730.

5 R. Li, B. Hu, T. Yu, Z. Shao, Y. Wang, S. Song, *Small Methods*, 2021, **5**, 2100246.

6 Y. Yang, H. Yao, Z. Yu, S. M. Islam, H. He, M. Yuan, Y. Yue, K. Xu, W. Hao, G. Sun, H. Li, S. Ma, P. Zapol, M. G. Kanatzidis, *J. Am. Chem. Soc.*, 2019, **141**, 10417.

7 L. Li, C. Sun, B. Shang, Q. Li, J. Lei, N. Li, F. Pan, *J. Mater. Chem. A.*, 2019, **7**, 18003-18011.

8 A. Sivanantham, P. Ganesan, S. Shanmugam, *Adv. Funct. Mater.*, 2016, **26**, 4661-4672.

9 H. Liu, X. Ma, Y. Rao, Y. Liu, J. Liu, L. Wang, M. Wu, *ACS Appl. Mater. Interfaces.*, 2018, **10**, 10890-10897.

10 F. Du, L. Shi, Y. Zhang, T. Li, J. Wang, G. Wen, A. Alsaedi, T. Hayat, Y. Zhou, Z. Zou, *Appl.Catal. B.*, 2019, **253**, 246-252.

11 T. Kou, T. Smart, B. Yao, I. Chen, D. Thota, Y. Ping, Y. Li, *Adv. Energy Mater.*, 2018, **8**, 1703538.

12 T. Zhu, L. Zhu, J. Wang, G.W. Ho, *J. Mater. Chem. A.*, 2016, **4**, 13916-13922.

13 J. Liu, J. Wang, B. Zhang, Y. Ruan, L. Lv, X. Ji, K. Xu, L. Miao, J. Jiang, *ACS Appl. Mater. Interfaces*, 2017, **9**, 15364-15372.

14 X. Xiao, L. Tao, M. Li, X. Lv, D. Huang, X. Jiang, H. Pan, M. Wang, Y. Shen, *Chem. Sci.*, 2018, **9**, 1970-1975.

15 K. Ao, D. Li, Y. Yao, P. Lv, Y. Cai, Q. Wei, *Electrochim. Acta*, 2018, **264**, 157-165.

16 Y. Li, B. Zhang, W. Wang, X. Shi, J. Zhang, R. Wang, B. He, Q. Wang, J. Jiang, Y. Gong, H. Wang, *Chem. Eng. J.*, 2021, **405**, 126981.

17 Y. Wu, Y. Wang, Z. Wang, X. Li, *J. Mater. Chem. A.*, 2021, **9**, 23574-23581.

18 J. Zhang, Z. Zhang, Y. Ji, J. Yang, K. Fan, X. Ma, C. Wang, R. Shu, Y. Chen, *Appl. Catal. B.*, 2021, **282**, 119609.

19 T.L.L. Doan, D.C. Nguyen, S. Prabhakaran, D.H. Kim, D.T. Tran, N.H. Kim, J.H. Lee, *Adv. Funct. Mater.*, 2021, **31**, 2100233.

20 Y. Pan, K. Sun, Y. Lin, X. Cao, Y. Cheng, S. Liu, L. Zeng, W.-C. Cheong, D. Zhao, K. Wu, Z. Liu, Y. Liu, D. Wang, Q. Peng, C. Chen, Y. Li, *Nano Energy*, 2019, **56**, 411-419.

21 Z.F. Huang, J. Song, K. Li, M. Tahir, Y.T. Wang, L. Pan, L. Wang, X. Zhang, J.J. Zou, *J. Am. Chem. Soc.*, 2016, **138**, 1359-1365.

22 Z. Chen, R. Wu, Y. Liu, Y. Ha, Y. Guo, D. Sun, M. Liu, F. Fang, *Adv. Mater.*, 2018, **30**, 1802011.

23 Y. Li, S. Niu, D. Rakov, Y. Wang, M. Caban-Acevedo, S. Zheng, B. Song, P. Xu, *Nanoscale*, 2018, **10**, 7291-7297.

24 P. Ji, H. Jin, H. Xia, X. Luo, J. Zhu, Z. Pu, S. Mu, *ACS Appl. Mater. Interfaces*, 2020, **12**, 727-733.

25 Z. Pu, C. Zhang, I.S. Amiinu, W. Li, L. Wu, S. Mu, *ACS Appl. Mater. Interfaces*, 2017, **9**, 16187-16193.

26 X. Liu, B. Wen, R. Guo, J. Meng, Z. Liu, W. Yang, C. Niu, Q. Li, L. Mai, *Nanoscale*, 2018, **10**, 9856-9861.

27 H. Xue, A. Meng, H. Zhang, Y. Lin, Z. Li, C. Wang, *Nano Res.*, 2021, **14**, 4173-4181.

28 T. Liu, X. Ma, D. Liu, S. Hao, G. Du, Y. Ma, A.M. Asiri, X. Sun, L. Chen, *ACS Catal.*, 2016, **7**, 98-102.

29 Y. Sun, Z. Xue, Q. Liu, Y. Jia, Y. Li, K. Liu, Y. Lin, M. Liu, G. Li, C.Y. Su, *Nat. Commun.*, 2021, **12**, 1369.